Journal of Physics: Conference Series **2667** (2023) 012065 doi:10.1088/1742-6596/2667/1/012065

Phase space analysis of the 3-level Lipkin-Meshkov-Glick model using parity adapted U(D)-spin coherent states

A Mayorgas[1], J Guerrero[3] and M Calixto[1,2]

[1] Department of Applied Mathematics and [2] Institute Carlos I of Theoretical and Computational Physics, University of Granada, Fuentenueva s/n, 18071 Granada, Spain
[3] Department of Mathematics, University of Jaen, Campus Las Lagunillas s/n, 23071 Jaen, Spain

E-mail: albmayrey97@ugr.es

Abstract. We study the phase-space properties of the 3-level Lipkin-Meshkov-Glick as paradigmatic case of critical, parity symmetric, N-quDit systems undergoing a quantum phase transition in the thermodynamic limit $N \to \infty$. We generalize U(2) spin coherent states to U(D) (quDits), and define the coherent state representation Q_ψ (Husimi function) of a symmetric N-quDit state $|\psi\rangle$ in the phase space $\mathbb{C}P^{D-1} = \mathrm{U}(D)/[\mathrm{U}(1) \times \mathrm{U}(D-1)]$. This allows us to define parity adapted U(D) coherent states (𝔠-DCATs), which reproduce accurately the lowest energy Hamiltonian eigenstates obtained by numerical diagonalization. We visualize precursors of the QPTs by plotting localization measures (Husimi function and its moments) of the parity adapted U(D) coherent states and the numerical Hamiltonian eigenstates for a finite number of particles.

1. Introduction

Phase space and information statistical methods are useful to describe quantum phase transitions (QPTs), as in the Anderson metal-insulator transition [1]. They are also an important method in quantum optics, connecting quantum and statistical mechanics through coherent states (CSs) [2, 3]. In this article, we study the generalization from Heisenberg-Weyl CSs to U(D)-spin CSs (DSCSs for short), in order to deal with D-level quantum systems or quDits [4]. DSCSs provide complex analytical representations of quantum states and operators, where the Husimi function plays the role of phase-space quasi-probability distribution function [5]. In our case, the quDits phase space will be associated to the coset space $\mathrm{U}(D)/[\mathrm{U}(1) \times \mathrm{U}(D-1)] = \mathbb{C}P^{D-1}$, a complex projective space that generalizes the Bloch sphere and that is linked to the totally symmetric representation of U(D) [6]. At the same time, we redefine the concept of moments of the Husimi function in the phase-space $\mathbb{C}P^{D-1}$ to measure the localization of the quantum states [7]. The moments are good indicators of QPTs in critical quantum systems, such as Bose-Einstein condensates [8], the Dicke model [9], and the LMG model [10]. The generalization of this methods to multi-quDits systems give us a more complex and richer structure than using the traditional Heisenberg -Weyl group or U(2). Indeed, the parity symmetry group $\mathbb{Z}_2$ appearing in the spontaneous symmetry breaking of 2-level QPTs, now turn into $\mathbb{Z}_2^{D-1}$ for D-level systems [11].

2. D-level LMG model

The 3-level LMG model is a particular case of a second quantized Hamiltonian describing pairing correlations

$$H_D = \sum_{i=0}^{D-1}\sum_{\mu=1}^{N} \varepsilon_i c^\dagger_{i\mu} c_{i\mu} - \sum_{i,j,k,l=0}^{D-1}\sum_{\mu,\nu=1}^{N} \lambda^{kl}_{ij} c^\dagger_{i\mu} c_{j\mu} c^\dagger_{k\nu} c_{l\nu} \tag{1}$$

where μ denotes N identical particles distributes among D energy levels labeled by i. The two-body residual interactions (with strength λ) scatter pairs of particles between the D levels (total number of particles=const.). If we consider the following list of assumptions,

- Define U(D) "quasispin" collective operators $S_{ij} = \sum_{\mu=1}^{N} c^\dagger_{i\mu} c_{j\mu}$.
- Vanishing interactions in the same level and equal interactions in different levels.
- Dividing two-body interactions by the number of particle pairs $N(N-1)$ to make the Hamiltonian an intensive quantity (energy density).
- Same energy spacing between levels $\varepsilon_i = \varepsilon$.

We arrive to the simplified version of the previous Hamiltonian,

$$H_D = \frac{\epsilon}{N}(S_{D-1,D-1} - S_{00}) - \frac{\lambda}{N(N-1)} \sum_{i\neq j=0}^{D-1} S^2_{ij}\,. \tag{2}$$

which is called the D-level LMG Hamiltonian. We shall also restrict to indistinguishable atoms, so that we use the fully symmetric irreducible representations of U(D). Hence, the Hilbert space is spanned by the Bose-Einstein-Fock states $|\vec{n}\rangle = \frac{(a_0^\dagger)^{n_0}\ldots(a_{D-1}^\dagger)^{n_{D-1}}}{\sqrt{n_0!\ldots n_{D-1}!}}|\vec{0}\rangle$.

The interaction codified in the Hamiltonian (2) only scatters pairs of particles, thus there is a conserved quantity, the parity $\Pi_i = \exp(\mathrm{i}\pi S_{ii})$ of the population S_{ii} in each level $i = 0,\ldots,D-1$. The energy eigenstates have discrete parity symmetry $\mathbb{Z}_2^{D-1} = \mathbb{Z}_2 \times \overset{D-1}{\ldots} \times \mathbb{Z}_2$, as $\Pi_0 = (-1)^N \Pi_1 \ldots \Pi_{D-1}$. This parity will be spontaneously broken in the thermodynamic limit $N \to \infty$, leading to a highly degenerated ground state. The elements of $\mathbb{Z}_2^{D-1}$ are labeled by the strings $\mathbb{b} = [b_1,\ldots,b_{D-1}] \in \{0,1\}^{D-1}$, and the elements of the Pontryagin dual $\widehat{\mathbb{Z}_2^{D-1}} \sim \mathbb{Z}_2^{D-1}$ by $\mathbb{c} = [c_1,\ldots,c_{D-1}] \in \{0,1\}^{D-1}$. Therefore, $\mathbb{c}$ label the 2^{D-1} parity invariant subspaces, whose projectors are

$$\Pi_{\mathbb{c}} = 2^{1-D} \sum_{\mathbb{b}\in\{0,1\}^{D-1}} (-1)^{\mathbb{c}\cdot\mathbb{b}} \Pi^{\mathbb{b}}\,, \tag{3}$$

where $\mathbb{c}\cdot\mathbb{b} = c_1 b_1 + \cdots + c_{D-1} b_{D-1}$ and $\Pi^{\mathbb{b}} \equiv \Pi_1^{b_1} \ldots \Pi_{D-1}^{b_{D-1}}$.

3. U(D)-spin coherent states and adaptation to parity

In order to study the LMG model spectrum, we shall study the U(D)-spin coherent states (DSCS for short), which are good variational states reproducing the ground state of the LMG model in the thermodynamic limit $N \to \infty$. We define DSCS à la Perelomov [4],

$$|\boldsymbol{z}\rangle^{(N)} = \frac{1}{\sqrt{N!}} \left(\frac{a_0^\dagger + z_1 a_1^\dagger + \cdots + z_{D-1} a_{D-1}^\dagger}{\sqrt{1 + |z_1|^2 + \cdots + |z_{D-1}|^2}} \right)^N |\vec{0}\rangle, \tag{4}$$

where $\boldsymbol{z} = (z_1,\ldots,z_{D-1})$ are coordinates in a patch of the projective manifold $\mathbb{C}P^{D-1} = \mathrm{U}(D)/[\mathrm{U}(1)\times\mathrm{U}(D-1)]$, where $i=0$ is the reference level. The coefficients of the DSCS in the Fock basis are $c_{\vec{n}}(\boldsymbol{z}) = \sqrt{\frac{N!}{\prod_{i=0}^{D-1} n_i!}} \frac{\prod_{i=1}^{D-1} z_i^{n_i}}{(1+\boldsymbol{z}^\dagger\boldsymbol{z})^{N/2}}$, with the scalar product $\boldsymbol{z}^\dagger\boldsymbol{z} = |z_1|^2 + \cdots + |z_{D-1}|^2$.

They are not orthogonal $\langle \boldsymbol{z}|\boldsymbol{z}'\rangle = \frac{(1+\boldsymbol{z}^\dagger\boldsymbol{z}')^N}{(1+\boldsymbol{z}^\dagger\boldsymbol{z})^{N/2}(1+\boldsymbol{z}'^\dagger\boldsymbol{z}')^{N/2}}$ and define an overcomplete set of states $1 = \int_{\mathbb{C}^{D-1}} |\boldsymbol{z}\rangle\langle\boldsymbol{z}| d\mu(\boldsymbol{z})$ with the Haar measure $d\mu(\boldsymbol{z}) = \frac{(D-1)!}{\pi^{D-1}}\binom{N+D-1}{N}\frac{d^2z_1 \ldots d^2z_{D-1}}{(1+\boldsymbol{z}^\dagger\boldsymbol{z})^D}$.

As DSCS do not display the parity symmetry $\mathbb{Z}_2^{D-1}$, we have to create a parity adaptation of them on invariant subspaces $\Pi_{\mathbb{c}}$ for finite N, called $\mathbb{c}$-DCAT states, so as to have variational states apart from in the thermodynamic limit. $\mathbb{c}$-DCAT states are defined as

$$|\boldsymbol{z}\rangle_{\mathbb{c}} \equiv \frac{\Pi_{\mathbb{c}}|\boldsymbol{z}\rangle}{\mathcal{N}(\boldsymbol{z})_{\mathbb{c}}} = \frac{2^{1-D}}{\mathcal{N}(\boldsymbol{z})_{\mathbb{c}}} \sum_{\mathbb{b}\in\{0,1\}^{D-1}} (-1)^{\mathbb{c}\cdot\mathbb{b}} |\boldsymbol{z}\rangle^{\mathbb{b}} \tag{5}$$

where $|\boldsymbol{z}\rangle^{\mathbb{b}} = \Pi^{\mathbb{b}}|\boldsymbol{z}\rangle = |((-1)^{b_1}z_1, \ldots, (-1)^{b_{D-1}}z_{D-1})$ and the normalization constant is $\mathcal{N}(\boldsymbol{z})^2_{\mathbb{c}} = 2^{1-D}\frac{\sum_{\mathbb{b}}(-1)^{\mathbb{c}\cdot\mathbb{b}}(1+\boldsymbol{z}^\dagger\boldsymbol{z}^{\mathbb{b}})^N}{(1+\boldsymbol{z}^\dagger\boldsymbol{z})^N}$. For instance, for $D = 2$ levels $\mathbb{c} = [c_1] \in \big\{[0], [1]\big\}$, we obtain the well known Schrödinger cat as superposition of two states

$$|z\rangle_\pm = \frac{|z\rangle \pm |-z\rangle}{\sqrt{2\pm 2\left(\frac{1-|z|^2}{1+|z|^2}\right)^N}}\,, \tag{6}$$

where $|\boldsymbol{z}\rangle_{[0]} = |\boldsymbol{z}\rangle_+$, $|\boldsymbol{z}\rangle_{[1]} = |\boldsymbol{z}\rangle_-$. In the case of $D = 3$ levels, the parity label is $\mathbb{c} = [c_1, c_2] \in \big\{[0,0], [0,1], [1,0], [1,1]\big\}$, and the $\mathbb{c}$-3CAT is

$$|\boldsymbol{z}\rangle_{\mathbb{c}} = \tfrac{1}{4\mathcal{N}(\boldsymbol{z})_{\mathbb{c}}}\Big[\,|(z_1,z_2)\rangle + (-1)^{c_1}|(-z_1,z_2)\rangle + (-1)^{c_2}|(z_1,-z_2)\rangle + (-1)^{c_1+c_2}|(-z_1,-z_2)\rangle\Big]. \tag{7}$$

The $\mathbb{c}$-DCAT definition is problematic as it leads to $\Pi_{\mathbb{c}}|\boldsymbol{z}\rangle = 0$ and $\mathcal{N}(\boldsymbol{z})_{\mathbb{c}} = 0$ when $c_i = 1$ and $z_i = 0$. Therefore, the expression (5) contains an indeterminate form of type "0/0", which can be avoided using limits. For example, in the case $D = 2$ in equation, in the odd parity case there is an indetermination (6),

$$\lim_{z\to 0}|z\rangle_{[1]} = \lim_{z\to 0}\frac{|z\rangle - |-z\rangle}{\sqrt{2-2\left(\frac{1-|z|^2}{1+|z|^2}\right)^N}} = \lim_{z\to 0}\frac{\left(\frac{2\sqrt{N}}{\sqrt{(N-1)!}}z(a_0^\dagger)^{N-1}a_1^\dagger + O(z^2)\right)|\vec{0}\rangle}{2\sqrt{N}z + O(z^2)} = |n_0{=}N{-}1, n_1{=}1\rangle\,. \tag{8}$$

For $D = 3$ level in equation (7), we have

$$\lim_{z_1\to 0}|\boldsymbol{z}\rangle^{(N)}_{\mathbb{c}} = (a_1^\dagger)^{c_1}|(0,z_2)\rangle^{(N-c_1)}_{[c_2]}\,, \quad |(0,z_2)\rangle_{[c_2]}\propto\Pi_{[c_2]}|(0,z_2)\rangle \quad \text{reduced } [c_2]\text{-3CAT}, \tag{9}$$

$$\lim_{z_2\to 0}|\boldsymbol{z}\rangle^{(N)}_{\mathbb{c}} = (a_2^\dagger)^{c_2}|(z_1,0)\rangle^{(N-c_2)}_{[c_1]}\,, \quad |(z_1,0)\rangle_{[c_1]}\propto\Pi_{[c_1]}|(z_1,0)\rangle \quad \text{reduced } [c_1]\text{-3CAT}, \tag{10}$$

$$\lim_{z_1,z_2\to 0}|\boldsymbol{z}\rangle^{(N)}_{\mathbb{c}} = |n_0{=}N{-}c_1{-}c_2, n_1{=}c_1, n_2{=}c_2\rangle \quad \text{Fock basis state.} \tag{11}$$

In the general D case, it is convenient to define a set of null coordinates $\boldsymbol{z}_L = \{z_{i_1}, \ldots, z_{i_l}\}$, l non-repeated indexes $L = \{i_1, \ldots, i_l\}$, which will tend to 0, and a set of non-zero coordinates $\boldsymbol{z}_K = \{z_{j_1}, \ldots, z_{j_k}\}$, k non-repeated indexes $K = \{j_1, \ldots, j_k\}$. With this notation, the vector $\boldsymbol{z} = (\boldsymbol{z}_K, \boldsymbol{z}_L) = (z_1, \ldots, z_{D-1})$ contains all the $k + l = D - 1$ projective coordinates, and the limit of the $\mathbb{c}$-DCAT is

$$\lim_{z_L\to\mathbf{0}_L}|\boldsymbol{z}\rangle^{(N)}_{\mathbb{c}} = \underbrace{(a_{i_1}^\dagger)^{c_{i_1}}\ldots(a_{i_l}^\dagger)^{c_{i_l}}}_{\substack{\text{levels } n_{i_1}=c_{i_1},\ldots,n_{i_l}=c_{i_l}\\ \|\mathbb{c}_L\|_0 \text{ particles}\\ \mathbb{c}_L=[c_{i_1},\ldots,c_{i_l}]\in\mathbb{Z}_2^l \text{ parity}}} \underbrace{|(\boldsymbol{z}_K, \boldsymbol{z}_L = \mathbf{0}_L)\rangle^{(N-\|\mathbb{c}_L\|_0)}_{\mathbb{c}_K}}_{\substack{\text{reduced } \mathbb{c}_K\text{-DCAT}\\ N-\|\mathbb{c}_L\|_0 \text{ particles}\\ \mathbb{c}_K=[c_{j_1},\ldots,c_{j_k}]\in\mathbb{Z}_2^k \text{ parity}}}, \tag{12}$$

where $\|\mathbb{c}_L\|_0$ is the 0-norm. In general, when we have more than one projective coordinates in $\boldsymbol{z}$, if we take the limit to 0 of some of them, we will obtain a reduced parity DCAT, and if we take the limit of all the coordinates, we will arrive to a Fock basis state. All these limits will be useful when differentiating the different phases of the LMG model.

4. 3-level LMG model and its quantum phase transitions at $N \to \infty$

The 3-level LMG Hamiltonian density is a particular case of the equation (2),

$$H = \frac{\epsilon}{N}(S_{22} - S_{00}) - \frac{\lambda}{N(N-1)} \sum_{i \neq j=0}^{2} S_{ij}^2 \,, \tag{13}$$

where λ is the control parameter which measures the interaction strength. We shall follow the standard procedure to study quantum phase transitions (QPT) in the thermodynamic limit $N \to \infty$ given by [12]. Firstly, we calculate the energy surface of the Hamiltonian (13), which is the coherent state expectation value of the Hamiltonian density in the thermodynamic limit,

$$E_{|\boldsymbol{z}\rangle}(\epsilon, \lambda) = \lim_{N\to\infty} \langle \boldsymbol{z}|H|\boldsymbol{z}\rangle = \epsilon \frac{|z_2|^2 - 1}{|z_1| + |z_2|^2 + 1} - \lambda \frac{z_1^2\left(\bar{z}_2^2 + 1\right) + z_2^2 + \text{c.c.}}{\left(|z_1| + |z_2|^2 + 1\right)^2}. \tag{14}$$

The calculation above relies in the fact that DSCS are good variational states which faithfully reproduce the ground state energy of Hamiltonian models in the limit $N \to \infty$. According to the equation (14), we will handle a four dimensional phase space $(z_1, z_2) \in \mathbb{C}^2$. Secondly, we calculate the variational minimum energy in the phase space parameters,

$$E^{(0)}(\epsilon, \lambda) = \min_{z_1, z_2 \in \mathbb{C}} E_{|(z_1, z_2)\rangle}(\epsilon, \lambda) = \begin{cases} -\epsilon, & 0 \leq \lambda \leq \frac{\epsilon}{2}, \quad \text{(I)} \\ -\frac{(2\lambda+\epsilon)^2}{8\lambda}, & \frac{\epsilon}{2} \leq \lambda \leq \frac{3\epsilon}{2}, \quad \text{(II)} \\ -\frac{4\lambda^2+3\epsilon^2}{6\lambda}, & \lambda \geq \frac{3\epsilon}{2}. \quad \text{(III)} \end{cases} \tag{15}$$

This is the variational ground state energy, which denote three different phases in the model depending on the values of the control parameter λ. In fact, there are two 2nd-order QPTs at $\lambda^{(0)}_{\text{I}\leftrightarrow\text{II}} = \epsilon/2$ and $\lambda^{(0)}_{\text{II}\leftrightarrow\text{III}} = 3\epsilon/2$. The critical values of z_1 and z_2 which make the energy minimum are real numbers,

$$z^{(0)}_{1\pm}(\epsilon, \lambda) = \pm \begin{cases} 0, & 0 \leq \lambda \leq \frac{\epsilon}{2}, \\ \sqrt{\frac{2\lambda-\epsilon}{2\lambda+\epsilon}}, & \frac{\epsilon}{2} \leq \lambda \leq \frac{3\epsilon}{2}, \\ \sqrt{\frac{2\lambda}{2\lambda+3\epsilon}}, & \lambda \geq \frac{3\epsilon}{2}, \end{cases} \qquad z^{(0)}_{2\pm}(\epsilon, \lambda) = \pm \begin{cases} 0, & 0 \leq \lambda \leq \frac{3\epsilon}{2}, \\ \sqrt{\frac{2\lambda-3\epsilon}{2\lambda+3\epsilon}}, & \lambda \geq \frac{3\epsilon}{2}. \end{cases} \tag{16}$$

The variational ground state (GS) is degenerated due to the four possible combinations of critical values $|z^{(0)}_{1\pm}, z^{(0)}_{2\pm}\rangle$, which implies that the $\mathbb{Z}_2^2$ parity symmetry of the Hamiltonian is broken. In general, the ground state degeneracy would go as 2^k, with k the number of nonzero components of $\boldsymbol{z}^{(0)} = (z^{(0)}_1, z^{(0)}_2)$. To restore GS parity, we project the GS with $\Pi_{[0,0]}$ (see (3)) and renormalize, so that the GS will acquire the form of a even parity 3CAT.

5. Numerical low-lying Hamiltonian eigenstates and fidelity with variational cats

The spectrum of the 3-level LMG Hamiltonian calculated numerically is a good starting point to check the accuracy of the variational calculations of the previous section. Therefore, in Figure 1 we present the numerical/exact energy densities of the Hamiltonian (13) as a function of the control parameter λ and for $N = 20$ particles. The solid colored lines represent the lowest energy eigenstates which have a definite $\mathbb{c}$-parity for all $\lambda \in (0, 3)$, $\langle\psi_0|\Pi_{[0,0]}|\psi_0\rangle = 1$, $\langle\psi_1|\Pi_{[1,0]}|\psi_1\rangle = 1$, $\langle\psi_3|\Pi_{[0,1]}|\psi_3\rangle = 1$, $\langle\psi_5|\Pi_{[1,1]}|\psi_5\rangle = 1$. In vertical grid lines, we have plot the values of λ where the QPTs occur in (15), which are also present in the numerical calculations as the colored lines degenerate close to $\lambda = 1/2$ and $\lambda = 3/2$. We take $\epsilon = 1$ from now on for the sake of simplicity. The degeneracy in the ground state for finite N can be seen as a precursor of the QPT for

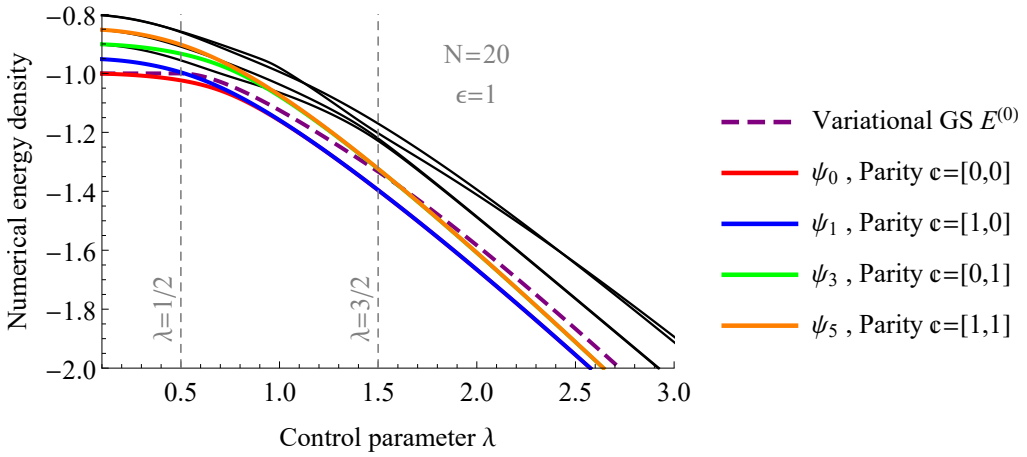

Figure 1. In solid colored lines, the numerical energy densities of the first eigenstates of the Hamiltonian (13) as a function of the control parameter λ and for $N = 20$ particles. In solid black lines, the rest of the eigenenergies, and in dashed purple, the variational GS (15). The vertical grid lines represent the quantum phase transitions (15).

$N \to \infty$. The variational GS, plotted in a dashed purple line, has an energy density close to the numerical one and will improve when increasing N in the numerical calculations.

The natural extension of the variational approach of Section 4 for the excited states and a finite number of particles N is as follows. Firstly, we create a parity adapted U(3) CSs (or 𝕔-3CATs), $|\boldsymbol{z}\rangle_{\mathbb{c}} \equiv \frac{\Pi_{\mathbb{c}}|\boldsymbol{z}\rangle}{\mathcal{N}(\boldsymbol{z})_{\mathbb{c}}}$. Then, we substitute one of the four critical coherent state parameters combinations $\boldsymbol{z}^{(0)} = (z_{1+}^{(0)}, z_{2+}^{(0)})$ (obtained for $N \to \infty$ in eq.(16)) into $|\boldsymbol{z}\rangle_{\mathbb{c}}$, that is $|\boldsymbol{z}^{(0)}\rangle_{\mathbb{c}} = \lim_{\boldsymbol{z}\to\boldsymbol{z}^{(0)}} |\boldsymbol{z}\rangle_{\mathbb{c}}$. We compare via fidelity how good is this new variational approximation, that is we calculate the overlap of the variational excited states $|\boldsymbol{z}^{(0)}\rangle_{\mathbb{c}}$ with the numerical ones $|\psi_i(\lambda)\rangle$. The fidelity $\left|{}_{\mathbb{c}}\langle \boldsymbol{z}^{(0)}|\psi_i(\lambda)\rangle\right|$ is in general close to one for all the values of λ which are not close to the critical ones, that is, the variational states $|\boldsymbol{z}^{(0)}\rangle_{\mathbb{c}}$ fail to reproduce the numerical eigenstates near the QPTs. This variational procedure for finite N can be improved maximizing the overlap $|{}_{\mathbb{c}}\langle \boldsymbol{z}|\psi_i(\lambda)\rangle|^2 = \mathcal{N}(\boldsymbol{z})_{\mathbb{c}}^2 Q_{\psi_i(\lambda)}(\boldsymbol{z})$ in phase space $\boldsymbol{z} = (z_1, z_2)$, and defining new variational states as 𝕔-3CATs $|\boldsymbol{z}\rangle_{\mathbb{c}}$ evaluated in the $\boldsymbol{z}$ of the minimization (see reference [13] for a complete discussion).

6. Husimi function and localization measures in phase space $\mathbb{C}P^{D-1}$

The DSCS studied in Section 3 provide a phase space representations of wave functions in quantum physics. In particular, we are going to focus in the Husimi function, its moments, and inverse participation ratio (IPR). The Husimi function in the phase space $\mathbb{C}P^{D-1}$ of a quantum states $|\psi\rangle$ is defined as its overlap with a DSCS, $Q_\psi(\boldsymbol{z}) = |\langle \boldsymbol{z}|\psi\rangle|^2$, with the normalization $\int_{\mathbb{C}^{D-1}} Q_\psi(\boldsymbol{z}) d\mu(\boldsymbol{z}) = 1$. The Husimi function of a DSCS is the overlap $Q_{|\boldsymbol{z}\rangle}(\boldsymbol{z}') = |\langle \boldsymbol{z}'|\boldsymbol{z}\rangle|^2$, and the Husimi function of a 𝕔-DCAT is $Q_{|\boldsymbol{z}\rangle_{\mathbb{c}}}(\boldsymbol{z}') = |\langle \boldsymbol{z}'|\boldsymbol{z}\rangle_{\mathbb{c}}|^2 = \frac{2^{1-D}\left|\sum_{\mathbb{b}}(-1)^{\mathbb{c}\cdot\mathbb{b}}(1+\boldsymbol{z}^\dagger \boldsymbol{z}'^{\mathbb{b}})^N\right|^2}{(1+\boldsymbol{z}'^\dagger \boldsymbol{z}')^N \sum_{\mathbb{b}}(-1)^{\mathbb{c}\cdot\mathbb{b}}(1+\boldsymbol{z}^\dagger \boldsymbol{z}^{\mathbb{b}})^N}$. We also define the ν-th moments of the Husimi function as

$$M_\nu(\psi) = \int_{\mathbb{C}^{D-1}} [Q_\psi(\boldsymbol{z})]^\nu d\mu(\boldsymbol{z}), \quad \nu > 1. \tag{17}$$

The 2nd moment $M_2(\psi)$ is called IPR, which is directly proportional to the localization of a state in the phase space. Note that the Lieb conjecture affirms that the states that maximize

the ν-th moments are the DSCSs [14],

$$\max_{\psi\in\mathcal{H}} M_\nu(\psi) = M_\nu(|\boldsymbol{z}\rangle) = \tfrac{(N+D-1)_{D-1}}{(N\nu+D-1)_{D-1}} \xrightarrow{N\to\infty} 1/\nu^{D-1}\,. \tag{18}$$

The ν-th moments of the $\mathbb{c}$-DCAT do not have a trivial expression and are calculated in [15]. In the case of the $\mathbb{c}$-3CAT, we present the thermodynamic limit of their ν-th moments,

$$\begin{aligned}\lim_{N\to\infty}\lim_{z_1,z_2\to 0} M_\nu(|\boldsymbol{z}\rangle_{\mathbb{c}}) &= \frac{(2^{c_1+c_2})^{1-\nu}}{\nu^{D-1}}, \quad \lim_{N\to\infty}\lim_{z_2\to 0} M_\nu(|\boldsymbol{z}\rangle_{\mathbb{c}}) = \frac{(2^{1+c_2})^{1-\nu}}{\nu^{D-1}} \quad \forall z_1\neq 0,\\ \lim_{N\to\infty} M_\nu(|\boldsymbol{z}\rangle_{\mathbb{c}}) &= \frac{(2^2)^{1-\nu}}{\nu^{D-1}} \quad \forall z_1, z_2\neq 0,\end{aligned} \tag{19}$$

where the numbers between parenthesis in the numerators are related with the number of humps of the Husimi function in phase space as we will see in the next section figures. The calculation of the thermodynamic limit of the ν-th moments of the $\mathbb{c}$-DCAT, together with the Lieb conjecture proof for U(D) and discussion of the Wehrl entropy, can be found in the reference [13].

7. Localization measures of the ground and first excited states

In this section, we gather all the necessary ingredients to achieve our main goal, to use localization measures in phase space (Husimi function and IPR) to analyze the QPT of the 3-level LMG model. In our variational model (14), the phase space is four dimensional, so we separate "position" $x_{1,2} = \mathrm{Re}(z'_{1,2})$ and "momentum" $p_{1,2} = \mathrm{Im}(z'_{1,2})$ coordinates to be able to plot the Husimi function $Q_{|\psi\rangle}(\boldsymbol{z}')$. In the left row of Figure 2, the Husimi function $Q_{|\boldsymbol{z}^{(0)}\rangle_{[0,0]}}(\boldsymbol{z}')$ of the variational GS is plotted for $N = 20$ particles. We can see how the number of humps of the Husimi function increases with the control parameter λ (going down in the same column), what is a sign of less localization in phase space due to the interaction. Indeed, we take values of λ inside the three different phases to display how the number of hump and the delocalization increases from top to the bottom row. The number of humps 2^k of the GS Husimi function is related to the parity $\mathbb{Z}_2^k$ of the variational GS in each different phase.

We can extend the LMG phase space analysis to the excited states, in particular, the three rows at right in Figure 2 shows the Husimi function of the variational excited states $Q_{|\boldsymbol{z}^{(0)}\rangle_{\mathbb{c}}}(\boldsymbol{z}')$ for $N = 20$ in "position" coordinates. Now we obtain a contour plot different to the variational GS one, due to the excited states Husimi function presents a number of humps

$$\#_{\text{humps}}\left(Q_{|\boldsymbol{z}^{(0)}\rangle_{\mathbb{c}}}(\boldsymbol{z}')\right) = 2^{\|\boldsymbol{z}^{(0)}\|_0+\|\mathbb{c}_L\|_0} \quad \forall N >> 1, \tag{20}$$

depending on the number of non-zero $\mathbb{c}$-3CAT coordinates $\|\boldsymbol{z}^{(0)}\|_0$ (which is a function of λ, see eq.(16)), and on the number of non-zero components $\|\mathbb{c}_L\|_0$ of the parity string $\mathbb{c}_L$, which contains the elements of $\mathbb{c}$ whose indexes match with ones of the null components of $\boldsymbol{z}^{(0)}$ (see reference [13] for more details).In phase III (bottom row in Figure 2), all the variational excited states has a similar structure to the GS, as it degenerates when increasing λ according to the energy spectrum in Figure 1.

The delocalization phenomena when increasing λ can be quantified using the IPR as in Figure 3. We plot the IPR of the, variational and numerical, GS and first excited states as a function of the control parameter. The variational results are more accurate than the numerical ones when comparing with the horizontal grid lines, which are the values of the variational states IPR in the thermodynamic limit (see eq.(19)), that is $\lim_{N\to\infty} M_2(|\boldsymbol{z}^{(0)}\rangle_{\mathbb{c}}) = \frac{(2^{c_1+c_2})^{-1}}{4}, \frac{(2^{1+c_2})^{-1}}{4}, \frac{(2^2)^{-1}}{4}$. This plot also agrees with Figure 2, as more IPR implies more localization, which happens when increasing λ. In addition, in phase III ($\lambda > 1.5$) all the states achieve the same value of the IPR as a sign of the GS degeneration.

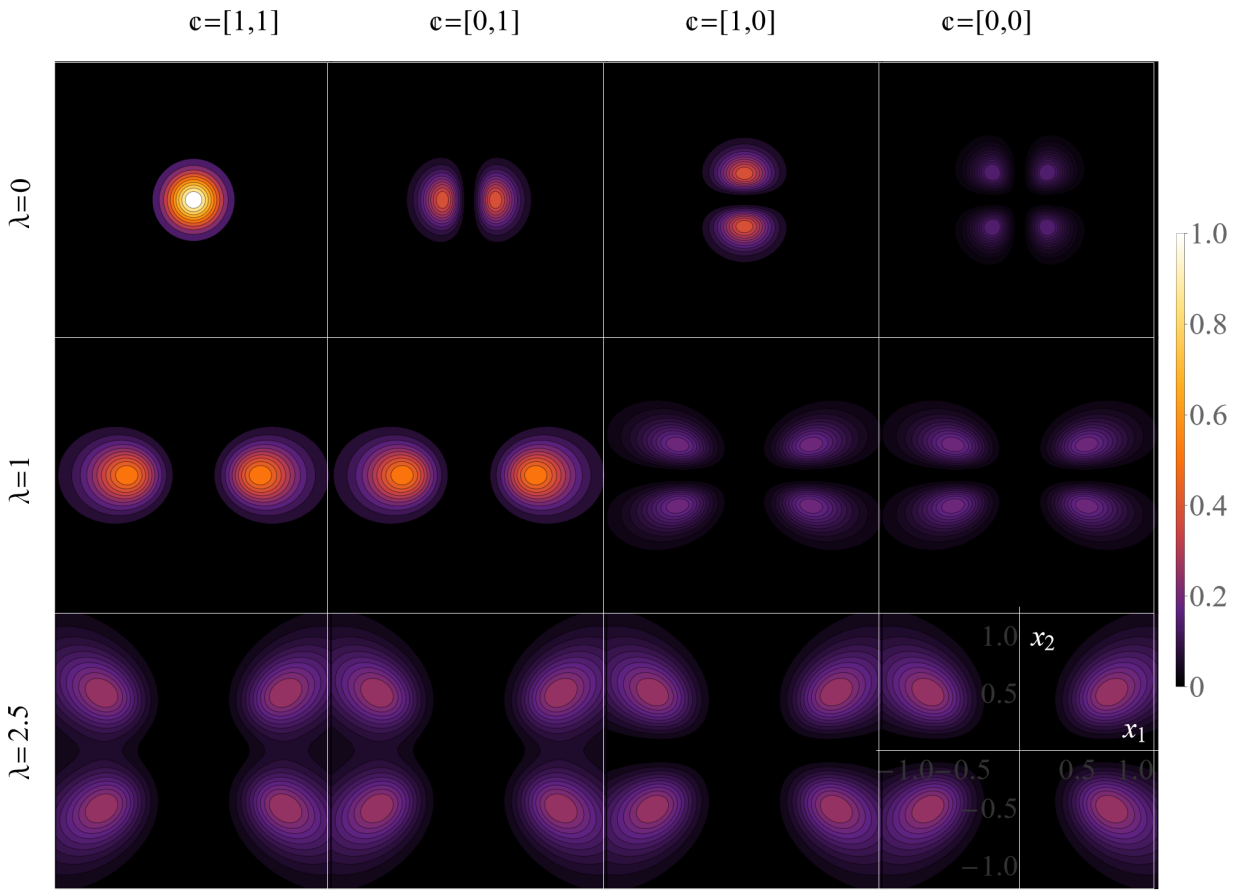

Figure 2. Contour plot of the Husimi function of the variational GS and first excited states in "position" phase space coordinates $x_{1,2} = \mathrm{Re}(z'_{1,2})$, for $N = 20$ particles and three different values of the control parameter λ in the three phases (15).

8. Conclusions

We have seen how the $\mathbb{Z}_2^{D-1}$ parity of the $\mathfrak{c}$-DCATs is reduced to $\mathbb{Z}_2^k$ when there are $l = D-1-k$ null projective coordinates. This fact allow us to extend previous studies of LMG U(3) ground states to excited states, which turn out to be modeled by $\mathfrak{c}$-3CATs of different parities (comparison via fidelity). We have proposed a definition of the Husimi function and its moments in the projective space $\mathbb{C}P^{D-1}$ using U(D) coherent states. These definitions fulfill the Lieb conjecture, as $\mathfrak{c}$-DCATs are less localized than DSCS in phase space (see eq.(18)). In particular, we have restricted the calculations to the three level case $D = 3$, where the QPTs of the LMG U(3) model are visualized in the phase space $\mathbb{C}P^2$ with the Husimi function, IPR, and Wehrl entropy of the GS. The control parameter λ have delimited the different phase, so an increment of λ is traduced in more humps in the GS Husimi function and less localization in phase space, together with an decrement of its IPR. The excited states also suffer delocalization in the QPT but depending on their $\mathfrak{c}$-parity. We propose for future work to extend the numerical calculations to $D > 3$ levels and check if the numerical eigenstates can be modeled by $\mathfrak{c}$-DCATs in general.

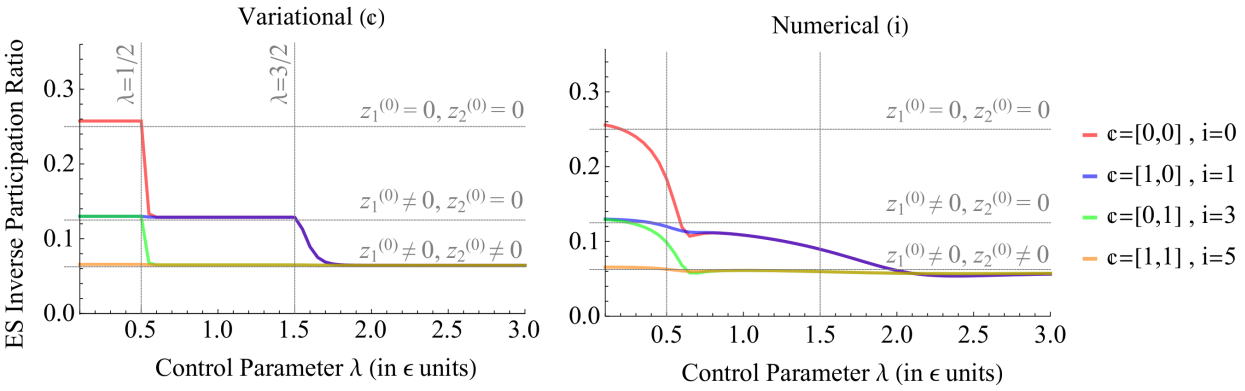

Figure 3. Inverse Participation Ratio of the numerical (bottom panel) and variational (top panel) excited states for $N = 50$ particles. The horizontal grid lines denote the thermodynamic limit of the IPR according to the eq.(19), and the vertical grid lines separate the different phases (15).

References

[1] Anderson P W 1958 *Phys. Rev.* **109**(5) 1492–1505 URL https://link.aps.org/doi/10.1103/PhysRev.109.1492
[2] Schleich W P 2001 *Quantum Optics in Phase Space* (Wiley-VCH Verlag Berlin GmbH) URL https://www.wiley.com/en-bo/Quantum+Optics+in+Phase+Space-p-9783527294350
[3] E F and Schroeck J 1996 *Quantum Mechanics on Phase Space* (Springer Netherlands) URL https://www.springer.com/gp/book/9780792337942
[4] Perelomov A 1986 *Generalized Coherent States and Their Applications* (Springer-Verlag Berlin Heidelberg) URL https://www.springer.com/gp/book/9783540159124
[5] Vourdas A 2006 *Journal of Physics A: Mathematical and General* **39** R65–R141 URL https://doi.org/10.1088/0305-4470/39/7/r01
[6] Calixto M, Mayorgas A and Guerrero J 2021 *Phys. Rev. E* **103**(1) 012116 URL https://link.aps.org/doi/10.1103/PhysRevE.103.012116
[7] Batistić B, Lozej i c v and Robnik M 2019 *Phys. Rev. E* **100**(6) 062208 URL https://link.aps.org/doi/10.1103/PhysRevE.100.062208
[8] Pérez-Campos C, González-Alonso J R, Castaños O and López-Peña R 2010 *Annals of Physics* **325** 325–344 ISSN 0003-4916 URL http://www.sciencedirect.com/science/article/pii/S0003491609001900
[9] Calixto M, del Real R and Romera E 2012 *Phys. Rev. A* **86**(3) 032508 URL https://link.aps.org/doi/10.1103/PhysRevA.86.032508
[10] Castaños O, López-Peña R, Hirsch J G and López-Moreno E 2006 *Phys. Rev. B* **74**(10) 104118 URL https://link.aps.org/doi/10.1103/PhysRevB.74.104118
[11] López-Peña R, Cordero S, Nahmad-Achar E and Castaños O 2015 *Physica Scripta* **90** 068016 URL https://doi.org/10.1088%2F0031-8949%2F90%2F6%2F068016
[12] Iachello F 2019 *Journal of Physics: Conference Series* **1194** 012048 URL https://dx.doi.org/10.1088/1742-6596/1194/1/012048
[13] Mayorgas A, Guerrero J and Calixto M 2023 *Phys. Rev. E* **108**(2) 024107 URL https://link.aps.org/doi/10.1103/PhysRevE.108.024107
[14] Lieb E H 1978 *Communications in Mathematical Physics* **62** 35–41 ISSN 1432-0916 URL https://doi.org/10.1007/BF01940328
[15] Sugita A 2003 *Journal of Physics A: Mathematical and General* **36** 9081–9103 URL https://doi.org/10.1088/0305-4470/36/34/310